Original Paper

UV light induced photoreduction in phosphate and fluoride-phosphate glasses doped with Ni^{2+}, Ta^{5+}, Pb^{2+}, and Ag^{+} compounds

Doris Möncke and Doris Ehrt

Otto-Schott-Institut für Glaschemie, Friedrich-Schiller-Universität Jena, Jena (Germany)

The photoreduction of polyvalent ions was studied in high purity fluoride-phosphate and metaphosphate glasses doped with Ni^{2+} ($3d^8$), Ta^{5+} ($5d^0$), Pb^{2+} ($6d^2$), and Ag^{+} ($3d^{10}$). Compared to the undoped base glasses all doped samples display different electronic transitions in the UV at the irradiation wavelength. Glass samples containing 50 to 5000 ppm dopants were irradiated with excimer lasers at 193 and 248 nm, respectively. The subsequent defect centers, formed at ppm levels, were characterized by EPR and optical UV-VIS spectroscopy.

The observed laser induced transmission losses in the UV and visible range increased in the order Ni, Ta, Pb to Ag. Extrinsic electron centers are formed by photoreduction of the dopants. $(Ni^{2+})^{-}$ is characterized by an optical transition with a maximum at 355 nm and an EPR signal around $g \approx 2.07$. The maxima of the optical transitions of the $(Pb^{2+})^{-}$-EC are positioned at 395 and 500 nm, of the $(Ta^{5+})^{-}$-EC at 465 nm. The photoionization products of silver depend strongly on the silver concentration. At a silver content of 50 ppm only the $(Ag^{+})^{-}$-EC is formed, visible in the optical spectra with a maximum around 450 nm. A second silver species, $(Ag^{+})_2^{-}$, which absorbs at 305 nm, is additionally observed in the sample doped with a silver concentration of 500 ppm. In the sample doped with 5000 ppm silver a third defect, the photooxidized $(Ag^{+})^{+}$-HC, with an optical band maximum at 405 nm and an EPR signal around $g \approx 2.3$ is observed as well.

The formation of extrinsic electron centers causes in all glasses an increase in the formation of intrinsic hole centers and often a decrease in the formation of intrinsic electron centers. Defect generation curves show that a very rapid darkening in the glasses is initiated by the addition of any of these dopants. The recovery rates of the defects formed depend strongly on the dopant, not on the glass matrix.

1. Introduction

UV radiation induced defects in glasses require high attention due to intensified applications of stronger lamps and lasers, working at increasingly shorter wavelengths. Solarization describes the effect of decreased transmission in the UV and VIS spectral range due to color centers generated by irradiation [1]. Color centers, or defects, evolve in ppm concentrations when the interaction of irradiation with the glass matrix is sufficient to ionize the glassy material. Defects consist of negatively charged electron centers (EC) and corresponding positively charged hole centers (HC). Many irradiation induced defect centers absorb strongly in the UV and VIS range, thus optical spectroscopy is a good tool for studying the formation of these defects [1 to 7]. Some of these defects are also paramagnetic, consequently EPR spectroscopy can yield much additional information on defects formed by irradiation [2 to 7].

Received 16 February 2004.

Presented in German at: 77th Annual Meeting of the German Society of Glass Technology (DGG) in Leipzig (Germany) on 28 May 2003.

Lead and silver are common dopants for photosensitive glasses [1 to 8] . The lead defect has been assigned either to a reduced "Pb^{+}" or an oxidized "Pb^{3+}" species [2, 7 to 9]. The transmission losses in silver doped glasses are attributed to a range of different Ag related defects species which have been characterized by either EPR or optical spectroscopy [6, 10 to 15]. Different kinds of Ni related defects have been seen for different glass systems. In borosilicate and silicate glasses with a higher optical basicity Ni^{2+} ($3d^8$) is photooxidized to $(Ni^{2+})^{+}$, in acidic glasses as fluoride phosphates or metaphosphate glasses, Ni^{2+} is on the other hand photoreduced to $(Ni^{2+})^{=}$ [6, 9, 10, 16 to 20]. Tantalum is no common dopant for glasses, though frequently used for coatings or in thin films. Experimental trials including different dopants proved the significant effect Ta^{5+} ($5d^0$) has on solarization, thus this ion was included in this study.

The UV cutoff between 230 and 250 nm in the glasses doped with 5000 ppm is caused by different electronic transitions of the doped ions. Due to the charge transfer (CT) transition of Fe^{3+}, the ever present impurity in these glasses, a substantial reduction of transmission around 250 nm is found even in those samples that contain only 50 ppm of the dopants. Although the UV edge is shifted towards lower

wavelengths in the low level doped glasses, the transmission is regularly reduced to less than 50 % at 250 nm whenever the 10 ppm iron impurities are present in the higher oxidation state [21].

The glass systems studied are a metaphosphate glass and a fluoride-phosphate (FP) glass. Both are characterized by a high transmission from the deep UV to infrared. The FP glasses exhibit other interesting properties for their application as laser and optical material, which include a low refractive index and an anomalous partial dispersion [22 and 23]. The kinetics of defect formation and recovery in undoped fluoride phosphate (FP) and phosphate glasses irradiated with lamps and lasers have been studied intensively before [24 and 25]. Numerous irradiation induced intrinsic defects in FP and phosphate glasses have been characterized by EPR and optical spectroscopy [23, 26 to 29]. The current knowledge on these intrinsic defects will be discussed in more detail in section 3.1. In general P related defects are much more stable than Frelated defects. The latter recover rapidly at room temperature and thus FP glasses are found to be more stable to solarization than phosphate glasses. Additionally irradiation at shorter wavelengths or higher energy causes an increased generation of defects as long as the sample UV cutoff is not positioned significantly beyond the wavelength of the radiation source employed. The addition of dopants often enhances the formation of defects considerably [1 to 4, 9, 18 to 20].

The predominant aim of this paper is the characterization of any extrinsic defects formed in the doped glasses by EPR and optical spectroscopy. Furthermore these extrinsic defects will be studied in regard to their thermodynamic and kinetic stability.

2. Experimental procedures

Batches of 100 to 300 g of the fluoride-phosphate glass FP10 (composition in mol%) 10 $Sr(PO_3)_2 \cdot 90$ (AlF_3, MgF_2, SrF_2, CaF_2) were melted in platinum crucibles in an electric furnace at 1000 °C. 250 g batches of the metaphosphate glass NSP (composition in mol%) 33 $NaPO_3 \cdot 67$ $Sr(PO_3)_2$ were melted in SiO_2 crucibles at 1200 °C for 90 min and for another 30 min at 1000 °C. The glasses were all cooled in graphite molds from 500 °C to room temperature with a cooling rate of about 30 K/h.

All model glasses were melted as undoped base glasses, doped with 50 to 5000 ppm of Ag (as $AgNO_3$), Ni (as $NiSO_4$), Pb (as PbF_2) and Ta (as Ta_2O_5). The reagents $NaPO_3$, $Sr(PO_3)_2$, AlF_3, SrF_2, CaF_2, and MgF_2 of high purity were used for the preparation; as a result, the iron content of the glasses could be kept as low as 5 to 10 ppm.

Polished plates 0.5 to 1 mm thick with dimensions of (10 × 20) mm^2 were irradiated with excimer lasers, an ArF laser working at 193 nm, and a KrF laser working at 248 nm. The pulse duration of both lasers was 20 ns and the power density of each pulse was 200 mJ/cm^2. The samples were irradiated in steps. The optical spectra were taken after 50, 250, 1000 and 3800 pulses or after 10, 100, 1000, 5500 and finally 10 000 pulses, respectively. This high pulse number ensured that defect formation reached the saturation level. Table 1 lists the irradiation setup for the differently doped glasses.

UV-VIS-NIR spectroscopy was used to characterize the glasses and to observe the irradiation induced defects. A double beam spectrophotometer (UV-3102 PC, Shimadzu, Tokyo (Japan)) was employed, recording the absorbance $A_\lambda = \lg(T_0/T)$ with an error < 1 % (T_0 and T: transmission without and with sample plate). The induced absorbance ΔA is used to describe the defects and is actually derived by subtraction of the spectra taken before irradiation from those taken after irradiation of the sample. As bulk contributions cancel out, this difference is equivalent to the optical spectrum of the induced defects alone.

A second independent analytical method, the electron paramagnetic resonance spectroscopy (EPR), was applied on the final irradiated samples. The EPR spectrometer used (ESP 300 E, Bruker, Karlsruhe (Germany)) worked with a frequency band of $\nu \approx 9.78$ GHz.

Recovery effects such as the recombination of induced defects over time were also studied. The optical spectra of the irradiated sample were taken at increasing time intervals after the irradiation process had been concluded. During this time all samples were stored in the dark at room temperature. The resolved Gaussian bands of the induced optical spectra were correlated with defect centers detected by EPR. Band separation of the diverse spectra was accomplished on the computer with customary software [30].

3. Results and discussion

Ni, Ta, Pb, and Ag are altogether polyvalent ions generally found in these glasses only in one oxidation state. The UV cutoff in the glasses doped with 5000 ppm is positioned below 250 nm for all glasses studied. The corresponding transmission spectra are shown in figures 1a to d. Although the cutoff should be shifted significantly to lower wavelengths in the glasses containing only 50 ppm of the dopants, a substantial absorption shoulder at 250 nm reduces the transmission near the UV cutoff in most glasses. This absorption is due to a charge transfer (CT) transition of $3d^5$ Fe^{3+} ions. While all glasses studied contain about 10 ppm iron impurities, strong variations are found in the Fe^{2+}/Fe^{3+} ratio between different melts [24 to 27].

The CT transition of the $3d^8Ni^{2+}$ ion lies below 240 nm. Much weaker d-d transitions of Ni^{2+} are also observed at 425 nm. Ta^{5+}, with its $5d^0$ electron configuration, exhibits a UV absorption edge at 245 nm also due to a CT transition [31]. In the lead doped glasses the transmission cutoff in the UV at 250 nm is shaped by the $s \rightarrow p$ transition of the $6s^2$ Pb^{2+} ion, while the $d \rightarrow s$ transition of the $5d^{10}$ Ag^+ ion determines the UV cutoff at 230 nm in the silver doped glass [1, 2 and 31]. Less common oxidation states of these dopants are Ni^0 and Ag^0, the latter absorbs around 450 nm. However these species are only detected when reducing melting conditions are applied or when the dopants are added at high concentrations [12 and 15].

Figures 1a to d also display the transmission spectra after laser irradiation. The doped glasses are all characterized by a significantly higher irradiation induced loss of transmission than the undoped base glass (figure 1c). The induced absorption increases from Ni^{2+} via Ta^{5+} and Pb^{2+}

Table 1. Composition of glasses, concentration of dopants and irradiation sources used

glass code	thickness d in mm	glass composition in mol%	dopants in ppm	laser*	λ in nm
FP10	1.0	10 % $Sr(PO_3)_2$ 90 % (AlF_3, SrF_2, CaF_2, MgF_2)	50 (Ni, Ta, Ag) 5000 (Ni, Pb, Ta)	ArF KrF	193 248
NSP	0.5	33 % $NaPO_3$ 67 % $Sr(PO_3)_2$	500 (Ag) 5000 (Pb, Ag)	KrF KrF	248 248

*) The lasers (up to 10^4 pulses) operated at < 15 Hz to prevent excessive thermal loading of the sample; the pulse length was 20 ns and the power density 200 mJ/cm^2 per pulse.

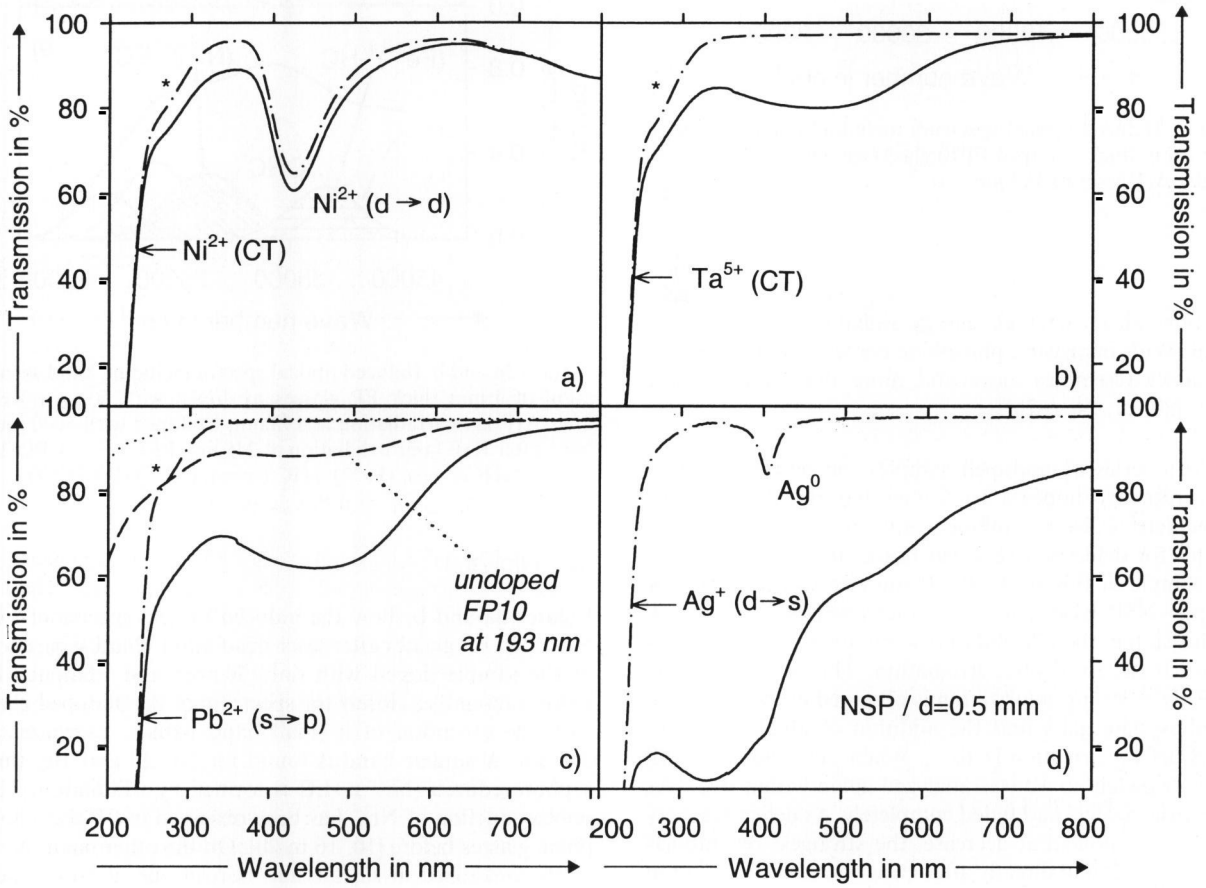

Figures 1a to d. Transmission spectra of samples before (·—·—) and after (——) irradiation to saturation level with the KrF laser at 248 nm: 1 mm thick FP10 glasses doped with 5000 ppm; a) Ni^{2+}, b) Ta^{5+}, c) Pb^{2+}, and d) 0.5 mm thick NSP glass doped with 5000 ppm Ag^+. Included in c): 1 mm thick undoped FP10 before (·····) and after (– – –) irradiation with the ArF laser at 193 nm. Iron impurities give rise to an Fe^{3+} CT transition around 250 nm (*).

to Ag^+ doped samples. All irradiation induced defects will be discussed in the order of increasing solarization, starting with the intrinsic defects observed in the undoped base glasses FP10 and NSP.

3.1 Intrinsic defects of the base glass

Several papers covering solarization in the same phosphate and FP glasses in more detail have been published in the past [18 to 20, 23 to 28]. It was shown that P-bonded defects are more stable than F-bonded defects. The latter cannot be observed at room temperature. As a result, fluoride-phosphate glasses show the same P-related intrinsic defects as phosphate glasses; however, with decreasing phosphate content FP glasses are progressively more stable to solarization.

Significant defect formation can be induced in phosphate glasses even with lamps and lasers of relatively low energy or respectively relatively high wavelengths. When high energy radiation like X-rays or a 193 nm laser is used, the induced absorbance in the phosphate glasses is several times stronger. Phosphate poor FP glasses might on the other hand be insensitive against a comparably low energy irradiation and nevertheless show a significant degree of so-

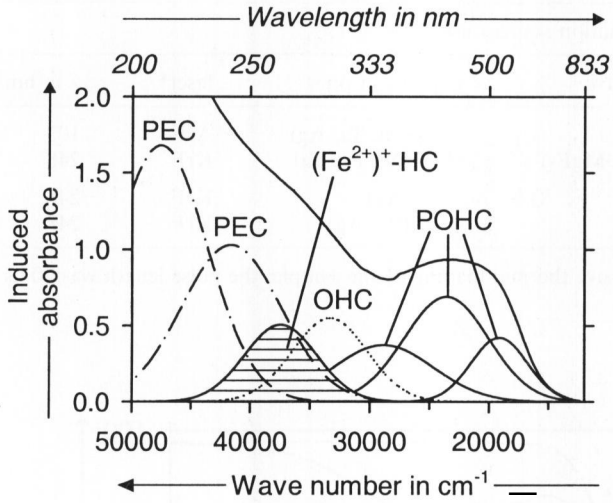

Figure 2. Induced optical spectrum including band separation of the 1 mm thick undoped FP10 glass (see figure 1c) irradiated with the ArF laser at 193 nm.

larization when the high energy radiation source is employed. With increasing phosphate content the behavior of FP glasses resembles more and more that of phosphate glasses [20, 21, 24 to 26].

For a series of undoped samples the reverse effect of defect recovery appears to follow the rule that readily formed defects also recombine readily. A surprisingly strong example for defect recovery was found after irradiating the NSP sample of this study at 248 nm (see section 3.4). The undoped NSP base glass is characterized by a very high transmission in the UV and only a minute decrease in transmission is observed after irradiation. This was surprising, especially as strong solarization is observed in the strontium metaphosphate glass and the addition of alkali often enhances defect formation [1 to 3]. When the irradiated NSP sample depicted above was analyzed again within five days all intrinsic defects had faded completely. As defect recovery follows an exponential decrease, the strongest recombination rates are found directly after cessation of the irradiation process. Therefore we must assume that most intrinsic defects recovered already before the optical spectra could be obtained and probably already during the irradiation process.

The difference spectrum of the undoped FP10 sample irradiated at 193 nm is displayed in figure 2. Typical defects are the phosphor oxygen bonded hole center (POHC) with three bands in the visible range between 330 and 600 nm, the oxygen hole center (OHC) at 300 nm, several phosphor related electron centers (PEC) near the UV, and the ubiquitous $(Fe^{2+})^+$-HC at 260 nm. Iron is an ever present impurity in glasses and Fe^{2+} is easily photooxidized to $(Fe^{2+})^+$ in FP as well as in phosphate glasses. The $(Fe^{2+})^+$-HC exhibits like Fe^{3+} a strong CT transition at 260 nm. This HC is very stable in these glasses and resists even thermal annealing to T_g, where otherwise all induced defects recover completely [26]. The same set of bands is found in phosphate glasses, although the band maxima are slightly shifted compared to the FP glasses.

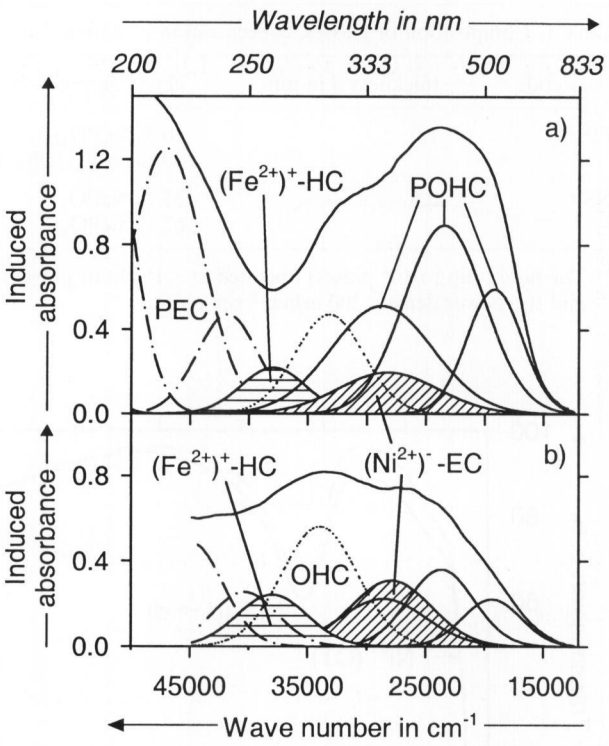

Figures 3a and b. Induced optical spectra including band separation of 1 mm thick FP glasses a) doped with 50 ppm Ni^{2+} after ArF laser irradiation at 193 nm; b) doped with 5000 ppm Ni^{2+} after KrF laser irradiation at 248 nm; PEC (·—·—), POHC (——), OHC (·····), $(Fe^{2+})^+$-HC (═══), (Ni^{2+})-EC (/////).

3.2 Nickel

Figures 3a and b show the induced optical spectra of two Ni doped FP glasses after laser irradiation. Band separation of the sample doped with only 50 ppm and irradiated at 193 nm resembles closely the spectrum of the undoped glass with the exception of a small band with a maximum at 355 nm. A similar band is found for Ni^+ [6 and 16], thus a photoreduced $(Ni^{2+})^-$-EC is formed by irradiation. The photoreduction of Ni^{2+} has been observed in FP and phosphate glasses before [10, 16 to 20]. On the other hand, Ni^{2+} is photooxidized in silicate and borosilicate glasses, which are characterized by a higher basicity than the FP glasses [20]. Bands of the typical intrinsic defects POHC, OHC and PEC are evident in figure 3a, just as one band with a maximum at 260 nm due to the photooxidized $(Fe^{2+})^+$-HC. The 248 nm laser induced optical spectrum of the same glass doped with 5000 ppm Ni (figure 3b) appears to have no resemblance to the spectrum of figure 3a. However, simulation of the spectrum turns out the same set of bands. The main difference is due to the significant increase of two bands, the $(Ni^{2+})^-$-EC at 355 nm and the OHC at 300 nm. Extrinsic defects may generally replace intrinsic defects of the same charge and/or may cause the additional formation of oppositely charged intrinsic defects. The formation of $(Ni^{2+})^-$-EC is accompanied by a selective increase of OHC. Further all intrinsic defects are formed in excess of those observed in the analogous irradiated undoped sample. The additional formation of intrinsic OHC agrees well with the assignment of the 355 nm band to an EC. This extrinsic EC can further be identified by EPR spectroscopy. The signal of the $(Ni^{2+})^-$-EC is characterized by g values between 2.0

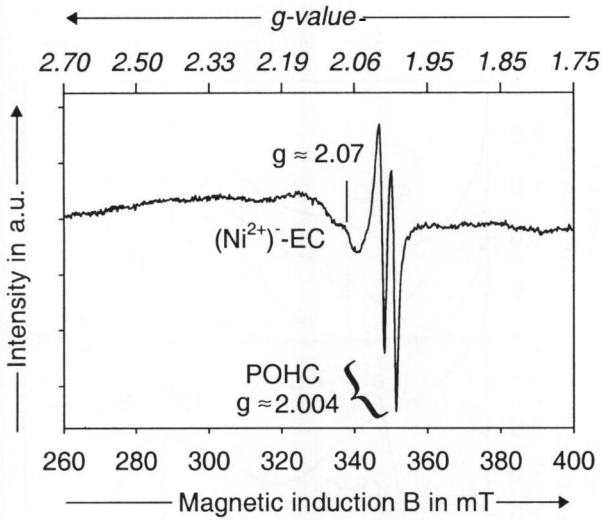

Figure 4. EPR spectrum of the FP10 sample doped with 5000 ppm Ni^{2+} irradiated with the KrF laser at 248 nm (sample of figure 3b).

and 2.5 [15, 18 to 20]. This agrees well with the EPR signal detected after irradiation with the 248 nm KrF laser in the FP10 sample doped with 5000 ppm Ni, which is displayed in figure 4.

Figures 5a to c display the generation curves of defect formation in undoped and with 50 ppm Ni doped FP10 after 193 nm ArF laser irradiation and of the glass doped with 5000 ppm Ni after 248 nm KrF laser irradiation. It is apparent that defect formation sets in much more rapidly when irradiated at 193 nm than at 248 nm and the saturation value is reached after a significantly smaller number of pulses with the ArF laser. Intrinsic defect formation would be lower in an undoped FP glass irradiated at 248 instead of 193 nm. However the concentration of dopants can compensate this effect, as the transmission losses in the glass doped with 5000 ppm Ni and irradiated at 248 nm are of similar magnitude than in the glass containing only 50 ppm Ni even though irradiated at 193 nm.

With the exception of the OHC defect, which is found to have a maximum induced absorbance of 0.5 in all glasses, the intensities of the different defects vary for all three glasses shown in figures 5a to c. Thus, the ratio of the intrinsic defects in the two glasses irradiated at 193 nm shift in favor of an increased formation of intrinsic HC in the Ni-doped glass, while intrinsic EC are generated in lower numbers. This shift is triggered by the formation of $(Ni^{2+})^{-}$-EC and becomes more selective in the glass doped with 5000 ppm Ni, where the OHC formation is favored over any of the other centers.

The two differently Ni doped glasses show also divergent recovery of effects. In the sample doped with 5000 ppm Ni a small increase of absorbance is observed around 350 nm where the Ni-EC and the OHC transitions are positioned. The absorption of the latter bands increases roughly by 25 %. At the same time even a small increase of transmission can be seen at longer wavelengths, where the POHC absorb. In the sample doped with 50 ppm Ni defect recovery is found over the whole wavelength region, as the transmission increases by roughly 10 %. Thus, a recombination of intrinsic HC with intrinsic EC and extrinsic Ni-EC is

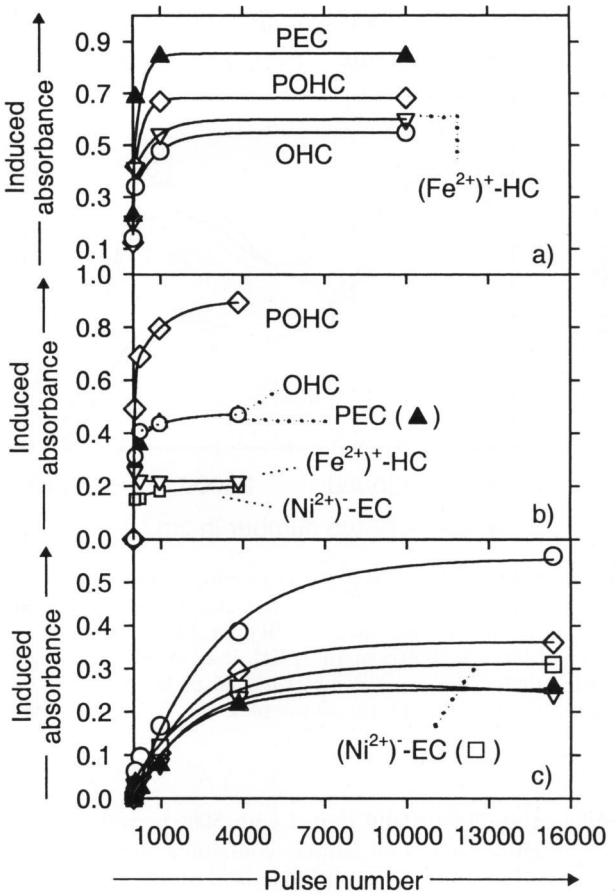

Figures 5a to c. Defect formation curves of: a) undoped FP10, ArF laser at 193 nm, b) FP10 doped with 50 ppm Ni^{2+}, ArF laser at 193 nm; c) FP10 doped with 5000 ppm Ni^{2+}, KrF laser at 248 nm. The maximum of induced absorbance of each defect is plotted versus the pulse number with: $(Fe^{2+})^{+}$-HC (▽), $(Ni^{2+})^{-}$-EC (□), PEC (▲), POHC (◇), OHC (○); the lines are included as guides to the eye only, d = 1 mm for all samples.

observed in the low level doped Ni glass, but a transformation of intrinsic PEC and POHC into OHC and extrinsic Ni-EC in the sample containing the higher Ni concentration.

3.3 Tantalum

Tantalum is probably present in the glasses investigated in the oxidation state +5. The CT transitions of Ta^{5+} ($5d^0$) are found in the UV and form the UV absorption edge [32 and 33]. The irradiation induced absorbencies of undoped FP10 and FP10 doped with 50 and 5000 ppm Ta respectively are displayed in figure 6. Compared to the undoped glass the induced absorbance in the visible range is almost twice as high in the doped glasses. Both samples irradiated at 193 nm, undoped and doped with 50 ppm Ta, show no significant differences in their spectra after irradiation when melted under air or remelted under reducing conditions. However, the influence of the melting conditions is fairly obvious in the glasses doped with 5000 ppm Ta and irradiated at 248 nm. The induced absorbance differs considerably with the melting conditions below 300 nm. At the same time the induced optical spectra of the samples ir-

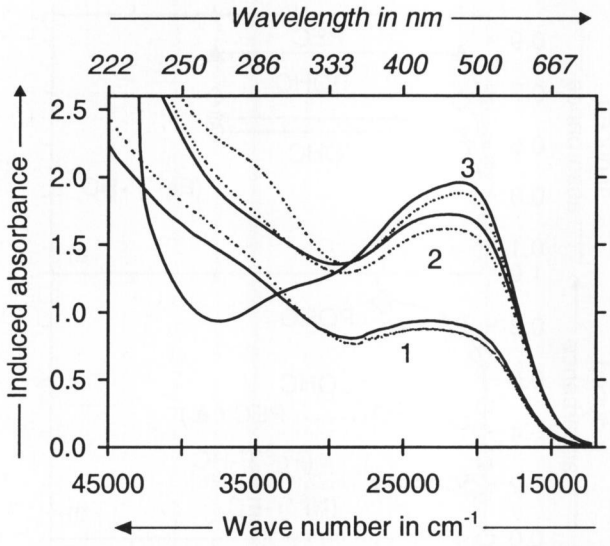

Figure 6. Induced optical spectra of undoped and Ta^{5+} doped FP10 samples after laser irradiation. Curve 1: undoped glasses, ArF laser at 193 nm; curve 2: 50 ppm Ta^{5+}, ArF laser at 193 nm; curve 3: 5000 ppm Ta^{5+}, KrF laser at 248 nm; samples melted under air (——), samples melted under reducing conditions (·····), d = 1 mm for all samples.

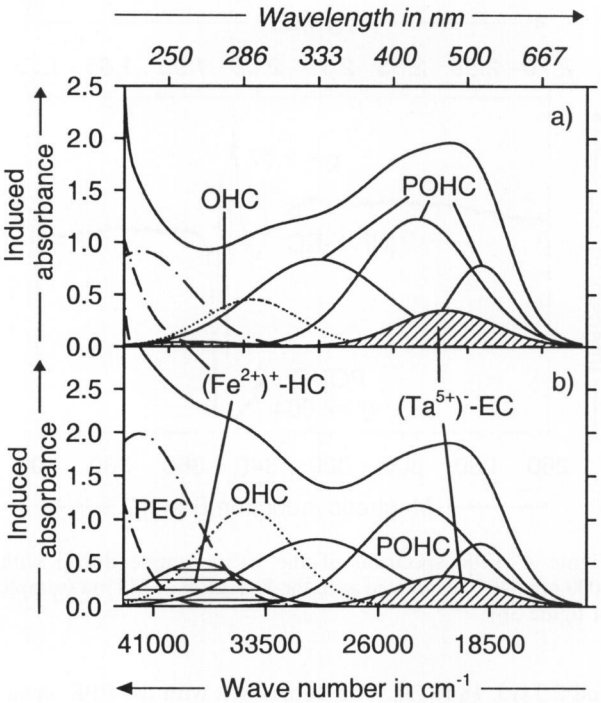

Figures 7a and b. Induced optical spectra including band separation of FP10 doped with 5000 ppm Ta^{5+} after irradiation with the KrF laser at 248 nm (curves 3 from figure 6): a) sample melted under air, $(Fe^{2+})^{+}$-HC ≈ 0.5 ppm; b) sample melted under reducing conditions, $(Fe^{2+})^{+}$-HC ≈ 3 ppm; PEC (·—·—), POHC (——), OHC (·····), $(Fe^{2+})^{+}$-HC (═══), $(Ta^{5+})^{-}$-EC (/////), d = 1 mm for all samples.

radiated at 248 nm and doped with 5000 ppm Ta diverge only slightly from those samples containing 50 ppm Ta and irradiated at 193 nm. Band separation of the induced absorbencies in the 5000 ppm containing glasses can be seen in figure 6. The band due to a $(Ta^{5+})^{-}$-EC is positioned around 450 nm. A similar band has been described for an inter valence charge transfer (IV-CT) transition between Ta^{4+} and Ta^{5+} in tantalum salt melts [32 and 33]. It still has to be determined if the band observed in the irradiated glasses is also caused by an IV-CT transition between Ta^{4+} and Ta^{5+} or if this band is due to an electron transition of Ta^{4+}, especially as this band is also observed in glasses doped only with 50 ppm Ta.

The intensity of the POHC and the $(Ta^{5+})^{-}$-EC in figures 7a and b is very similar in both glasses doped with 5000 ppm Ta, regardless of the melting conditions. The main differences in the spectra are positioned at lower wavelengths. Under reducing melting conditions most of the 10 ppm iron impurities is reduced to Fe^{2+} and thus the $(Fe^{2+})^{+}$-HC is formed by subsequent irradiation. Often 50 % of the iron ions are present as Fe^{3+} in FP glasses melted under air and without further oxidizing or reducing influence on the melt [21 and 27]. The Fe^{2+}/Fe^{3+} ratio can be shifted completely on the side of Fe^{2+} when melted under reducing conditions. In the sample doped with 5000 ppm tantalum most of the iron ions are found in the higher oxidation state so that contrary to the reduced melted sample and all the low level doped samples no Fe^{2+} ions are present for the irradiation induced oxidation to $(Fe^{2+})^{+}$.

The second difference in the two spectra of figures 7a and b is due to an intrinsic defect, the OHC at 300 nm. Not only the redox ratio, but also the glass matrix is influenced by the melting conditions, and as a result the kind and number of precursors may differ. Reducing melting conditions seem under certain conditions to increase the formation of OHC precursors in the FP glass matrix. The additionally

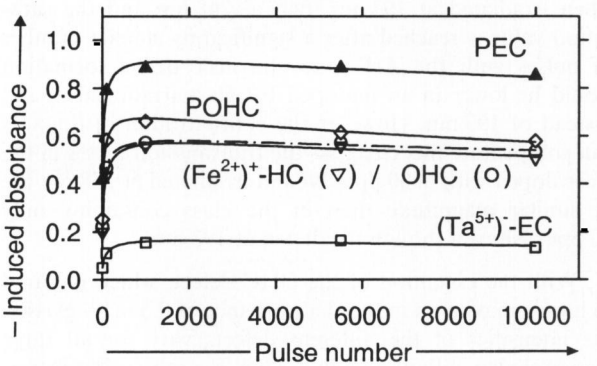

Figure 8. Defect formation curves of a 1 mm thick FP10 glass doped with 50 ppm Ta^{5+} (like curve 2 from figure 6). The maximum induced absorbance of the defects is plotted versus the pulse number with: PEC (▲), POHC (◇), OHC (○), $(Fe^{2+})^{+}$-HC (▽); $(Ta^{5+})^{-}$-EC (□); the lines are included as guides to the eye only.

observed increase in the formation of PEC in figure 7b goes in hand with the surplus OHC and $(Fe^{2+})^{+}$-HC formation.

Defect formation curves of FP10 doped with 50 ppm Ta melted under air and irradiated by the 193 nm ArF laser are displayed in figure 8. The maximally induced absorbance for the defects is already reached after application of the first 100 pulses. With ongoing irradiation even a slight decrease of the induced absorbance can be observed.

Within a year after ending the irradiation process an increase of transmission from about 60 to 70 % at 450 nm

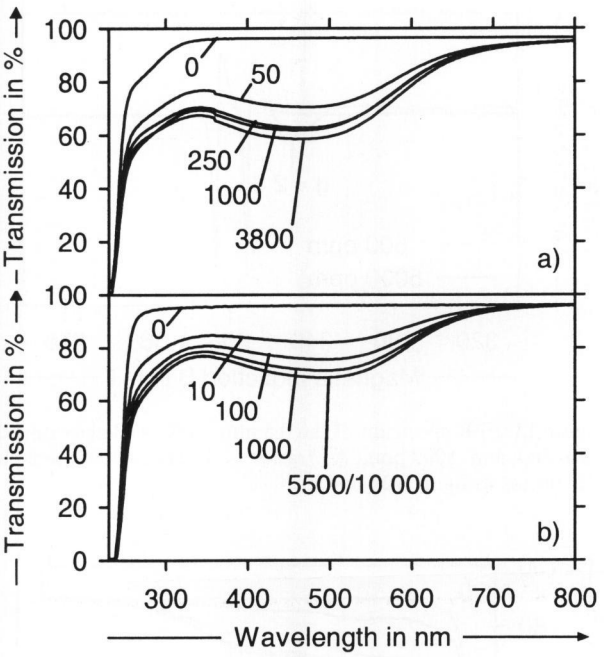

Figures 9a and b. Transmission spectra before irradiation (0 pulses) and with increasing pulse number of irradiation with the KrF laser at 248 nm in glass samples doped with 5000 ppm Pb^{2+}: a) 1 mm thick FP10 glass, and b) 0.5 mm thick NSP glass.

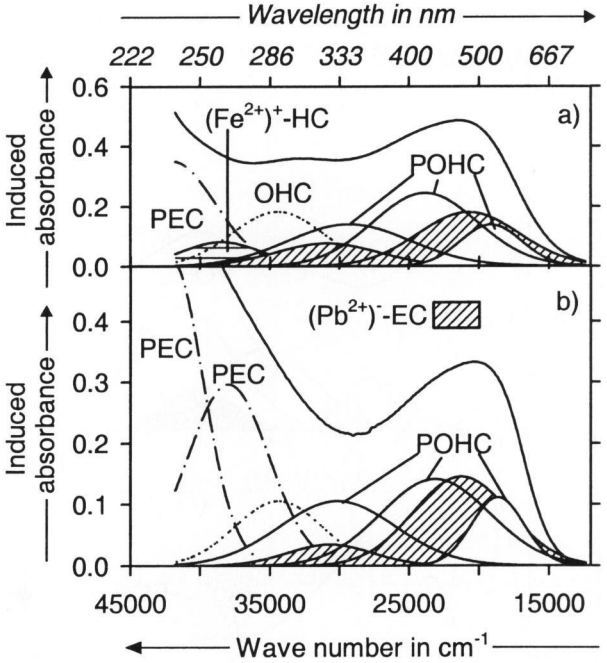

Figures 10a and b. Induced optical spectra including band separation of the two samples doped with 5000 ppm Pb^{2+} and irradiated with the KrF laser at 248 nm to the maximum pulse number as depicted in figures 9a and b: a) 1 mm thick FP10 glass; b) 0.5 mm thick NSP glass; PEC (·—·—); POHC (——); OHC (·····); $(Fe^{2+})^+$-HC (═); $(Pb^{2+})^-$-EC (/////).

can be observed for both, the 50 and the 5000 ppm doped FP10 glasses. As the recovery includes the whole wavelength range a general recombination including all kinds of intrinsic and extrinsic defects is proposed.

3.4 Lead

Very strong solarization effects are known for lead doped glasses. The photooxidation of Pb^{2+} to $(Pb^{2+})^+$-HC has been observed in silicate glasses. These are characterized by a higher optical basicity than the more ionic phosphate and FP glasses, where otherwise the photoreduction of Pb^{2+} to $(Pb^{2+})^-$-EC is known [1, 8, 34].

The transmission losses in FP10 and the NSP glasses doped with 5000 ppm Pb^{2+} and irradiated at 248 nm are shown in figures 9a and b. Band separations of the induced spectra of the two lead doped glasses are displayed in figures 10a and b. Two bands at 300 and 500 nm are needed for the fit in addition to the bands of the intrinsic defects. These bands are typical of the reduced Pb^+ species or the $(Pb^{2+})^-$-EC [1, 8, 34]. Intrinsic EC are also formed in significant amounts and the formation of intrinsic HC is correspondingly increased for charge balance reasons.

Remarkable are also the very strong recovery effects observed in the Pb doped glasses. The induced transmission after 10 000 pulses, where saturation of defect formation can be assumed, is displayed in figure 11 for the NSP sample. When this irradiated 0.5 mm thick sample was measured again several times over the following months, the transmission around 500 nm increases significantly from 40 to 60 %. The 1 mm thick FP10 sample even showed an increase of transmission from 30 to 60 % within the year after the irradiation process ended. As all wavelengths are affected

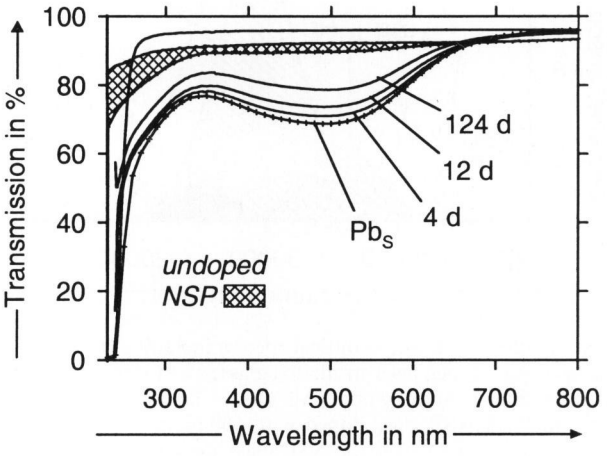

Figure 11. Transmission spectra of NSP glasses undoped and doped with 5000 ppm Pb^{2+} before irradiation (——) and after KrF laser irradiation at 248 nm with 10 000 pulses (+++) to the saturation level Pb_s. The recovery of the induced transmission losses of the Pb^{2+} doped glass is shown for the 4th, 12th and 124th day after the final irradiation. The induced transmission loss recovers completely after five days in the undoped NSP glass (×××).

by the recovery process, a general recombination of all defects is assumed.

3.5 Silver

Of the four dopants discussed in this paper, silver causes the strongest induced transmission losses. The solarization

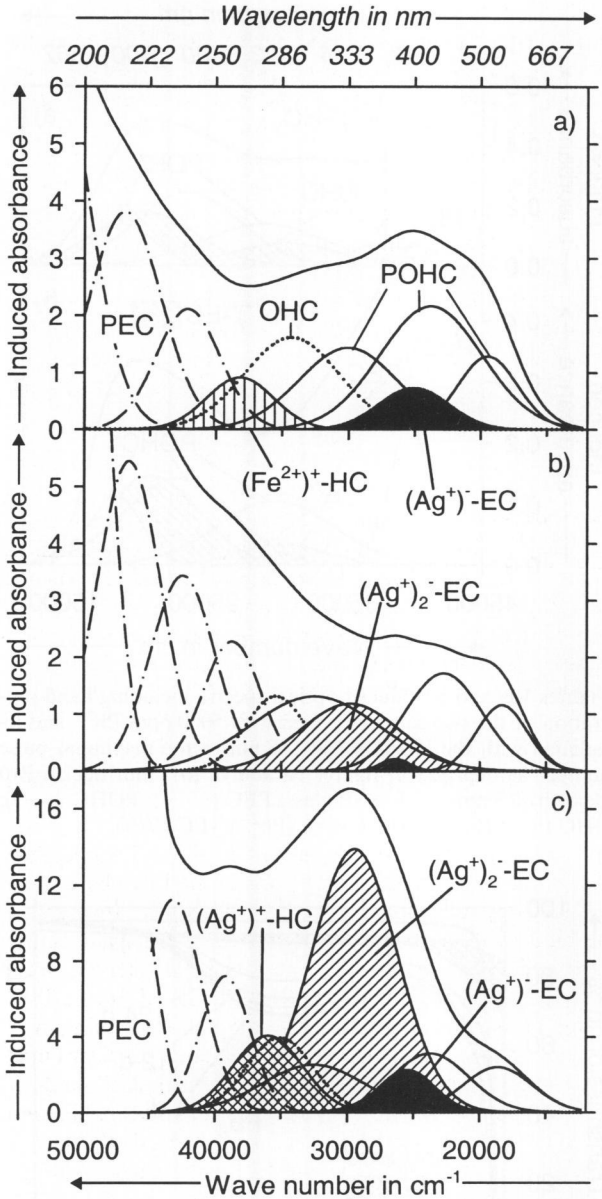

Figures 12a to c. Induced optical spectra including band separation of Ag^+ doped laser irradiated glasses; a) 1 mm thick FP10 sample doped with 50 ppm Ag^+, ArF laser at 193 nm, b) 0.5 mm thick NSP glass doped with 500 ppm Ag^+, KrF laser at 248 nm, c) 0.5 mm thick NSP glass doped with 5000 ppm Ag^+, KrF laser at 248 nm ← notice the higher intensity scale!.

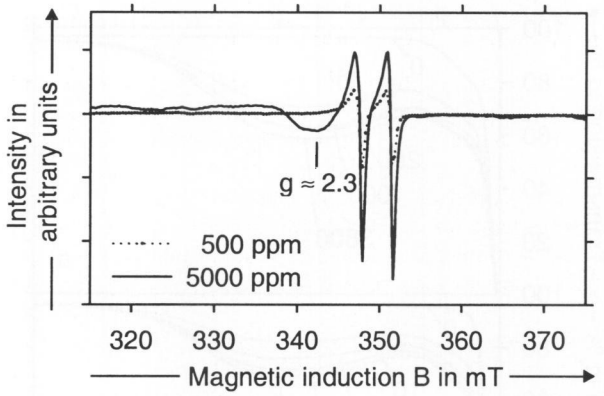

Figure 13. EPR spectrum of the 0.5 mm thick NSP glass doped with 500 and 5000 ppm Ag^+ after KrF laser irradiation at 248 nm (as in figure 12b and c).

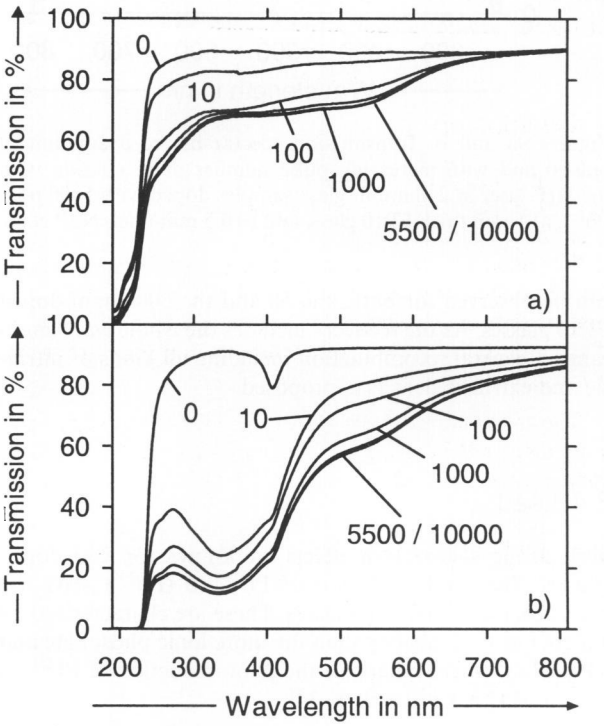

Figures 14a and b. Transmission spectra before irradiation (0 pulses) and with increasing pulse number of irradiation with the KrF laser at 248 nm of 0.5 mm thick NSP glasses doped with a) 500 ppm Ag^+ and b) 5000 ppm Ag^+.

effects depend strongly on the concentration of the dopant. The solubility of silver ions in these glasses is low and thus a small band due to colloidal elemental silver can be observed in figure 1d around 450 nm in the NSP glass doped with 5000 ppm Ag [14]. Silver ions are even less soluble in FP glasses, where colloidal silver segregates when added in concentrations exceeding 50 ppm.

Band separations of the induced spectra are shown in figures 12a to c. The induced spectrum of the FP10 glass doped with 50 ppm Ag is characterized by the known intrinsic bands and one additional band at 450 nm. In analogy to the Ag band seen in the glass containing the high silver concentration the newly induced band at 450 nm can be assigned to an $(Ag^+)^-$-EC. In the NSP glasses the induced bands of the intrinsic defects are slightly shifted compared to the FP glass. A second extrinsic defect at 350 nm is evident in the NSP glass doped with 500 ppm Ag. This band can be assigned to the $(Ag^+)_2^-$-EC in which two Ag^+ ions share the negative charge of one electron [6 and 12]. With increasing dopant concentration the latter defect becomes prominent as can be seen in figure 12c. In the spectrum of the glass doped with 5000 ppm Ag even a third band occurs at 275 nm. This band can be assigned to an $(Ag^+)^+$-HC which is also characterized by a strong EPR signal at $g \approx 2.3$ (figure 13) [6 and 15].

Figures 14a and b show the induced transmission losses of the silver doped NSP glasses with increasing pulse number. It is apparent that as before for Ta^{5+}, Ni^{2+} and Pb^{2+}

the main amount of induced defects is already formed within the first 100 or even the first 10 pulses.

The recovery effects in the NSP glass doped with 5000 ppm Ag^+ are less pronounced than those observed in the Pb^{2+} doped glass, but nevertheless extensive. Interestingly a transformation of defects is discernible in the high level Ag^+ doped glasses. In the 5000 ppm containing sample the transmission increases at most wavelengths with increasing storage time, but decreases around 300 nm where the $(Ag^+{}_2)^-$ species absorbs. A similar, slightly inferior recovery is observed in the NSP glass doped with 500 ppm Ag. The transmission increase is still smaller at 300 nm than at higher and lower wavelengths. In the FP10 glass doped with 50 ppm Ag a general increase of transmission by roughly 10 % can be observed at all wavelengths. No decrease in transmission around 300 nm was found. However, no such decrease would be expected in a sample where also no $(Ag^+{}_2)^-$ species had formed initially. As for the Pb^{2+} doped samples a general recombination of all defects is assumed for the low level Ag^+ doped FP10 glass.

4. Conclusion

Basically the glass matrix determines the nature and amount of intrinsic defects. FP glasses are more stable to solarization than NSP glasses. This is due to the instability of F-bonded defects and the intrinsic UV edge, which is shifted to shorter wavelengths in the FP glass. All doped samples showed increased solarization due to the formation of extrinsic defects, which often also enhance the formation of intrinsic defects.

The following extrinsic EC are formed for the four dopants discussed in this paper, which all have different electronic transitions in the UV:

$$Ni^{2+}\ (3d^8) \xrightarrow{h\nu} (Ni^{2+})^- + h^+,$$

$$Ta^{5+}\ (5d^0) \xrightarrow{h\nu} (Ta^{5+})^- + h^+,$$

$$Pb^{2+}\ (6s^2) \xrightarrow{h\nu} (Pb^{2+})^- + h^+,$$

$$Ag^+\ (3d^{10}) \xrightarrow{h\nu} (Ag^+)^- + h^+.$$

With increasing concentration of the Ag dopant two additional Ag related defects, a diatomic EC and an HC, are observed:

$$2Ag^+ \xrightarrow{h\nu} (Ag^+)_2^- + h^+,$$

$$Ag^+ \xrightarrow{h\nu} (Ag^+)^+ + e^-.$$

Intrinsic defects were replaced by newly formed extrinsic EC only to a small extent. More often a significant increase in the formation of intrinsic HC (OHC and POHC) balances the excess charge of the additionally formed extrinsic EC.

The melting conditions influence the nature of the precursors. As a result an increased formation of $(Fe^{2+})^+$-HC or OHC is observed in samples melted under reducing conditions.

The irradiation source, or in this study the laser wavelength, is also an important parameter which determines the quantity of the formed defects. In undoped glasses the lasers working at lower wavelengths and thus higher energy cause much stronger effects than those working at lower energies or longer wavelengths where the glasses show no intrinsic absorption. However, when irradiated at 248 nm the samples in this study contained a 100 times higher concentration of dopants than when irradiated at 193 nm, thus the UV cutoff was shifted to higher wavelengths. With higher dopant concentration more extrinsic defects are formed and the overall solarization increases as well. Thus, in combination the contrary influences of irradiation wavelength, initial absorbance, and dopant concentration cannot be separated.

The slope of the defect formation curves is steeper, and thus the pulse number needed to reach the saturation level much lower, after irradiation at 193 nm compared to irradiation at 248 nm. Addition of dopants often enhances overall defect formation. The saturation levels are reached more rapidly in doped than in undoped samples. For Ta an upper limit of defect formation is observed after irradiation of the first laser pulses and the induced absorbance decreases even by further irradiation. The $(Ni^{2+})^-$-EC is formed very promptly as well, like many extrinsic EC more rapidly than the intrinsic defects. The formation of certain intrinsic HC is also enhanced together with the formation of extrinsic EC.

Recovery effects are very strong in the NSP base glass and on the other hand relatively low in the FP10 base glass. The recovery rates of the doped glasses depend strongly on the kind of dopant and the influence of the glass matrix was negligible. Minor recovery effects characterized by a transmission increase around 10 % were found for the Ta^{5+} doped glasses, as well as for the 50 ppm containing Ag^+ and Ni^{2+} doped FP10 glasses. As the fading was distributed evenly over all wavelengths, a recombination of all kinds of observed defects can be assumed. A similar recombination of defects was observed for the Pb^{2+} doped glasses, although recovery resulted in these glasses in a twofold increase of transmission. In the NSP glasses doped with 500 and 5000 ppm Ag as well as in the FP10 sample doped with 5000 ppm Ni recovery was small and could be linked to the transformation of less stable defects into the very stable $(Ag^+)_2^-$- and $(Ni^{2+})^-$-EC.

*

The authors thank R. Atzrodt and A. Matthai for the sample preparation, M. Friedrich and B. Rambach for the EPR measurements, R. Marschall for the laser irradiation and the Deutsche Forschungsgemeinschaft for the financial support (EH 140/3).

5. References

[1] Weyl, W. A.: Coloured glasses. Sheffield: Society of Glass Technology, 1951.
[2] Bishay, A.: Radiation induced color centers in multicomponent glasses. J. Non-Cryst. Sol. **3** (1970) pp. 54–114.
[3] Wong, J.; Angell, C. A.: Glass structure by spectroscopy. New York et al.: Dekker, 1976.

[4] Friebele, E. J.: Radiation effects. In: Uhlmann D. R.; Kreidl, N. J. (eds.): Optical properties of glass. Westerville, OH: Am. Ceram. Soc., 1991. Pp. 205–262.
[5] Griscom, D. L.: Electron spin resonance in glasses. J. Non-Cryst. Sol. **40** (1980) Pp. 211–272.
[6] Brown, D. M.; Dainton, F. S.: Matrix isolation of unstable lower valency states of metal cations. Trans. Farad. Soc. **62** (1966) pp. 1139–1150.
[7] Friebele, E. J.; Tran, D. C.: Radiation effects in ZrF4 based glasses. J. Non-Cryst. Sol. **72** (1985) pp. 221–232.
[8] Hosono, H.; Kawazoe, H.; Kanazawa, T.: Coordination of Pb^{2+} in oxide glasses determined by ESR and properties of binary lead glasses. J. Ceram. Soc. Jpn. **90** (1982) pp. 544–551.
[9] Möncke, D.; Ehrt, D.: Irradiation induced defects in glasses resulting in the photoionization of polyvalent dopants. J. Opt. Mater. **25** (2004) pp. 425–437.
[10] Aleksandrov, A. I.; Bubnov, N. N.; Prokof'ev, A. I.: Stabilization of elements in unusual oxidation states and temperature-reversible dynamics of electron pairs in oxide glasses. EPR-investigation. Appl. Magn. Reson. **9** (1995) pp. 251–266.
[11] Treinin, A.: Trapped radicals in inorganic glasses. In: Kaiser, E. T.; Kevan, L. (eds.): Radical ions. New York: Wiley, 1968. Pp. 525–577.
[12] Paje, S. E., Garcia, M. A.; Llopis, J. et al.: Optical spectroscopy of silver ion-exchanged As-doped glass. J. Non-Cryst. Sol. **318** (2003) pp. 239–247.
[13] Pestryakov, A. N.; Davydov, A. A.: Study of supported silver states by the method of electron spectroscopy of diffuse reflectance. J. Electron Spec. Rel. Phen. **74** (1995) pp. 195–199.
[14] Bohren, C. F.; Huffman, D. R.: Absorption and scattering of light by small particles. New York: Wiley, 1998. Pp. 272–374.
[15] Feldmann, T., Treinin, A.: Inorganic radicals trapped in glasses at room temperature. IV. Silver radicals in metaphosphate glasses. J. Chem. Phys. **47** (1967) pp. 2754–2758.
[16] Buxton, G. V.; Sellers, R. M.: Pulse radiolysis study of M+ ions. J. Chem. Soc. Faraday Trans. **7** (1975) pp. 558–567.
[17] Amano, C.; Watanabe, T.; Fujiwara, S.: ESR of hot ions: Ni(I) complex ions produced in Ni(II) complexes by γ-irradiation. Bull. Chem. Soc. Jpn. **46** (1973) pp. 2586–2587.
[18] Möncke, D.; Ehrt, D.: Radiation induced defects in CoO and NiO doped fluoride-phosphate glasses. Glastech. Ber. Glass Sci. Technol. **74** (2001) no. 3, pp. 65–73.
[19] Möncke, D.; Ehrt, D.: Radiation induced defects in CoO and NiO doped glasses demonstrated on a metaphosphate glass. Glastech. Ber. Glass Sci. Technol. **74** (2001) no. 7, pp. 199–209.
[20] Möncke, D.; Ehrt, D.: Radiation-induced defects in CoO- and NiO-doped fluoride, phosphate, silicate and borosilicate glasses. Glastech. Ber. Glass Sci. Technol. **75** (2002) no. 5, pp. 243–253.
[21] Ehrt, D.: UV-absorption and radiation effects in different glasses doped with iron and tin in the ppm range. C. R. Chim. **5** (2002) pp. 679–692.
[22] Lucas, J.; Smektala, F.; Adam, J. L.: Review: Fluorine in optics. J. Fluorine Chem. **14** (2002) pp. 113–118.
[23] Ehrt D.: Fluoroaluminate glasses for lasers and amplifiers. Current Opinion in Solid State and Materials Science **7** (2003) pp. 135–141.
[24] Natura, U.; Ehrt, D.: Generation and healing behavior of radiation-induced optical absorption in fluoride phosphate glasses: the dependence on UV radiation sources and temperature. Nuc. Inst. Meth. Phys. Res. B **174** (2001) pp. 143–150.
[25] Natura, U.; Ehrt, D.: Modeling of excimer laser radiation induced defect generation in fluoride phosphate glasses. Nuc. Inst. Meth. Phys. Res. B **174** (2001) pp. 151–158.
[26] Ehrt, D.; Ebeling, P.; Natura, U.: UV transmission and radiation-induced defects in phosphate and fluoride-phosphate glasses. J. Non-Cryst. Solids **263 & 264** (2000) pp. 240–250.
[27] Ehrt, D.; Ebeling, P.; Natura, U. et al.: Redox equilibria and ultraviolet radiation induced defects in glasses. In: Proc. XIX International Congress on Glass, Edinburgh, 2001. Vol. 1. Inv. Papers. Pp. 84–93.
[28] Hosono, H.; Abe, Y.: ESR study of radiation induced paramagnetic defect centers localized on a phosphorus in binary phosphate glasses. J. Non-Cryst. Sol. **71** (1985) pp. 261–267.
[29] Ebeling, P.; Ehrt, D.; Friedrich, M.: X-ray induced effects in phosphate glasses. Opt. Mater. **2** (2002) pp. 101–111.
[30] PeakFit v. 4.0 Documentation. San Rafael, CA (USA); Erkrath, Germany: Jandel scientific software © 1995 AISN Software.
[31] Izumitani, T.; Hirota, S.: Absorption and dispersion of optical glass intrinsic absorption of glass in vacuum ultraviolet region. Wiss. Z. Friedrich-Schiller-Univ. Jena, Naturwiss. R. **32** (1983) pp. 227–237.
[32] Stöhr, U.; Freyland, W.: Intervalence charge transfer and electronic transport in molten salts containing tantalum and niobium complexes in mixed valency. PCCP **1** (1999) pp. 4383–4387.
[33] Bachtler, M.; Rockenberger, J.; Fraland, W. et al.: Electronic absorption spectra of reduction products of pentavalent niobium and tantalum in different alkali chlorides and oxychloride melts. J. Phys. Chem. **98** (1994) pp. 742–747.
[34] Möncke, D.; Ehrt, D.: Photoionization of As, Sb, Sn and Pb in metaphosphate glasses. J. Non-Cryst. Solids (2004) in press.

E504P005

Contact:

Doris Möncke
Otto-Schott-Institut für Glaschemie
Friedrich-Schiller-Universität Jena
Fraunhoferstraße 6
D-07743 Jena

E-mail: DorisMoencke@web.de